

Probing Access Resistance of Solid-State Nanopores with a Scanning-Probe Microscope Tip

Changbae Hyun, Ryan Rollings, and Jiali Li*

An apparatus that integrates solid-state nanopore ionic current measurement with a scanning-probe microscope is developed. When a micrometer-scale scanning-probe tip is near a voltage-biased nanometer-scale pore (10–100 nm), the tip partially blocks the flow of ions to the pore and increases the pore access resistance. The apparatus records the current blockage caused by the probe tip and the location of the tip simultaneously. By measuring the current blockage map near a nanopore as a function of the tip position in 3D space in salt solution, the relative pore resistance increases due to the tip and $\Delta R/R_0$ is estimated as a function of the tip location, nanopore geometry, and salt concentration. The amplitude of $\Delta R/R_0$ also depends on the ratio of the pore length to its radius as Ohm's law predicts. When the tip is very close to the pore surface, ≈ 10 nm, experiments show that $\Delta R/R_0$ depends on salt concentration as predicted by the Poisson and Nernst–Planck equations. Furthermore, the measurements show that $\Delta R/R_0$ goes to zero when the tip is about five times the pore diameter away from the center of the pore entrance. The results in this work not only demonstrate a way to probe the access resistance of nanopores experimentally; they also provide a way to locate the nanopore in salt solution, and open the door to future nanopore experiments for detecting single biomolecules attached to a probe tip.

1. Introduction

A voltage-biased nanopore can electronically detect individual biopolymers in their native environment. Protein nanopores suspended in lipid bilayers are capable of characterizing single DNA and RNA molecules.^[1–4] Solid-state nanopores (SSNs) fabricated from silicon nitride, silicon dioxide, or aluminum oxide have been used to detect DNA and proteins.^[5–7] When a nanometer scale pore in a thin insulating membrane is immersed in an electrolyte solution and a voltage is applied across the membrane, most of the voltage drop occurs inside the pore (**Figure 1a**). However, there should be an appreciable amount of voltage drop occurring at the immediate vicinity of the pore entrance and

exit, characterized by an access resistance, due to the electric field distribution extending beyond the physical limits of the pore (see the Supporting Information (SI), Figure S2a). When charged particles such as biomolecules are close to the pore, the particles will be first captured by the electric field near the pore and then forced to move through the pore by the electrostatic force.^[8–11] The capturing process is determined by the electric field distribution near the pore which is also characterized as access resistance.^[8–12] For monitoring nanopore resistance change based sensing devices, access resistance is an important parameter and it becomes a dominant component of the pore resistance as a pore gets thinner, as has been demonstrated in recent monolayer thin graphene nanopore experiments.^[13–15]

One of the obstacles for a nanopore-based device to reach the promised potential is that the translocation speed of biomolecules has been too fast to be well resolved.^[3,16,17] Another is that the electric field distribution or the access resistance near a nanopore is not well characterized experimentally. To overcome these problems, optical tweezers^[18–20] as well as magnetic tweezers^[21] have been used to control

Dr. C. Hyun, R. Rollings, Prof. J. Li
Physics Department
University of Arkansas
Fayetteville, AR 72701, USA
E-mail: jialili@uark.edu



DOI: 10.1002/sml.201101337

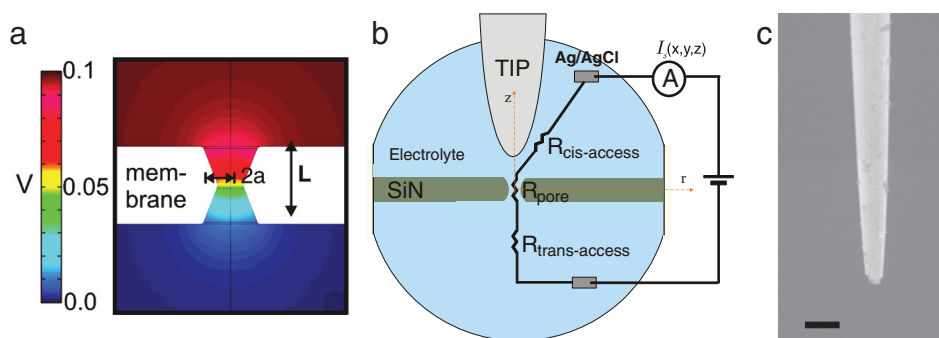


Figure 1. a) Simulation of electrical potential around a ≈ 100 nm diameter pore in 0.1 M KCl. The shape of the nanopore is idealized to a cylindrical hourglass shape based on recent work.^[12,37] b) Schematic drawing of nanopore ionic current profile measurement near a nanopore with the SSN-SPM system (not to scale). The measured total pore resistance is the sum of the pore resistance and the access resistances at both sides of the pore. The SPM tip close to the nanopore increases the access resistance in the *cis* chamber ($R_{\text{cis-access}}$). c) SEM image of a SPM tip used in this work. The scale bar is 5 μm .

DNA translocation through solid-state nanopores by attaching DNA molecules to micrometer size beads. Physical probes such as a focused laser beam,^[22] an electrolyte-filled micropipette,^[23,24] and a nanotube-attached scanning probe microscope (SPM) tip^[25] have been used to study the ionic conductance profile around solid-state nanopores. Motivated to reduce the positional fluctuation compared to optically trapped beads and to detect the controlled threading of single DNA molecules attached to a probe tip, we have designed and constructed a measuring system that integrates a solid-state nanopore with a scanning probe microscope (SSN-SPM), as shown in Figure 1b.

In the SSN-SPM system, the SPM tip (Figure 1b) has sub-nanometer scale position control with a piezo actuator. A scanning electron microscopy (SEM) image of a SPM tip used in this work is shown in Figure 1c. As illustrated in Figure 1b, the SSN-SPM system measures the ionic current, $I_s(x,y,z)$, through a nanopore as a SPM tip scans near the pore while keeping the tip height ($z = H_{\text{tip}}$) constant. The nanopores used in this work are fabricated in freestanding silicon nitride membranes by focused ion (Ga) beam (FIB) followed by low energy ion (noble gas) beam sculpting.^[5,26] The membrane divides the electrolyte solution into two sections: *cis* and *trans* chambers. Most electrolyte solutions used in the experiment contain 1 M potassium chloride (KCl) with 10 mM Tris at pH 8, with some solutions having lower KCl concentrations as specified. The sole electrical and fluidic connection between the two chambers is the nanopore. The ionic current through the pore is measured by a pair of Ag/AgCl electrodes in the chambers. The ionic current is measured and recorded with an Axopatch 200B integrated amplifier system (Molecular Devices). The chambers are mounted on the SPM sample stage. The relative position of the stage and probe are controlled by XYZ piezos.

1.1. Nanopore Resistance and Access Resistance

The total resistance of a nanopore (R_0) in salt solution includes the pore resistance (R_{pore}) inside the pore and the access resistance (R_{access}) from the entrances of the pore to the electrodes as shown in Figure 1b. Most features of the total resistance

can be modeled by assuming the pore is a radially symmetric cylinder with length L and diameter a , and that the electrode is infinitely far away. The concept of access resistance has been described by earlier publications.^[27,28] Assuming that the electrolyte is a homogeneous conducting medium with resistivity ρ , the total resistance can be written as

$$R_0 = R_{\text{pore}} + R_{\text{access}} = \frac{\rho L}{\pi a^2} + \frac{\rho}{2a} \quad (1)$$

The access resistance on one side of the membrane is $R_{\text{access}} = \rho/4a$, which is calculated by integrating the resistance from a disklike mouth to an infinite hemisphere.^[29] The access resistance has the same order of magnitude as the pore resistance if the pore length L is comparable to the pore radius a which is true for both protein and solid-state nanopores. According to Equation (1), the access resistance becomes the dominant component of the pore resistance when $L/a \leq 1.57$. Equation (1) considers the electrolyte as a homogeneous conducting medium. This is based on the assumption that the membrane and pore surfaces are uncharged. This assumption is good under the condition that the pore diameter is much larger than the Debye length. In this particular experiment, Equation (1) also assumes that the distance from the tip to the pore surface is much larger than the Debye length. For a given salt concentration and pH, a charged surface considerably reduces the access resistance of a channel,^[30] and the Poisson and Nernst–Planck (PNP) equations are needed to describe the flux of ions through charged channels.^[30,31]

The access resistance on one side of the pore, $R_{\text{access}} = \rho/4a$, is calculated assuming that there is no obstacle between the nanopore's mouth and the electrode and is based on Ohm's law. If we add obstacles close to the nanopore entrance, the access resistance contribution to the total resistance will increase. Using this principle, water-soluble polymers in the vicinity of the pore were used to study the access resistance contribution to the total nanopore channel resistance.^[9,32] A SPM tip near a nanopore entrance is a large obstacle that can partially block the ionic current flow and can generate a current blockage signal due to an increased pore access resistance. In this work, by measuring the ionic current blockage profile $I_s(x,y,z)$, we study how the relative pore resistance

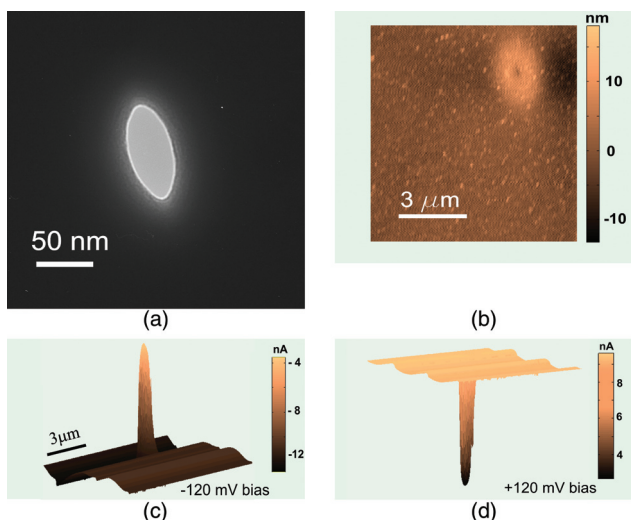


Figure 2. a) TEM image of an elliptical shape nanopore. The length of the major axis is 75 nm and the minor axis is 35 nm. b) Topography around the same nanopore as in (a) measured by an SPM tip. The bulge's major axis has the same orientation compared to the TEM image. c) Ionic current map around the nanopore recorded at $\psi = -120$ mV bias in a solution of 0.1 M KCl. d) Ionic current map measured with the same parameters as for (c) except that the polarity of the bias voltage is changed to $\psi = 120$ mV. The images of (b), (c), and (d) were measured simultaneously while a SPM tip was scanning, so the $x - y$ axis limits of (b), (c), and (d) are the same.

changes with the SPM tip position, nanopore diameter (D_p), and salt concentration.

2. Results and Discussion

2.1. Data Measured using the SSN-SPM System

Figure 2 shows a simultaneously measured topography and ionic current blockage profile as a SPM tip was scanning above a nanopore surface measured with the SSN-SPM system. An ellipse shaped nanopore was used in this measurement and its transmission electron microscope (TEM) image (Figure 2a) shows the pore had dimensions of 35 nm \times 75 nm. The amplitude of the oscillating tip is damped as it moves to within 30 nm of the surface. The shear force feedback system maintains the specific engaging distance between the tip and the surface. The engagement distance was set at $H_{\text{tip}} = 10$ nm for Figure 2b–d. The height feedback error in the SPM is estimated to be about ± 1 nm from the topography noise. The raster scanning speed of the tip was $3 \mu\text{m s}^{-1}$ over a $10 \mu\text{m} \times 10 \mu\text{m}$ surface. The topography of the nanopore (Figure 2b) shows a crater as reported previously.^[33] The crater has the elliptical shape as shown in Figure 2a.

The nanopore ionic current profile in Figure 2c was measured at $\psi = -120$ mV bias voltage across the Ag/AgCl electrodes in 100 mM KCl solution. In the current map, when the tip passes the pore, the ionic current amplitude is reduced from -10 to -4 nA. To verify that the current blockage is due to the tip interaction with the nanopore, we scanned the same area of Figure 2b with positive 120 mV bias voltage.

As expected, the ionic current dropped from 8 to 3 nA as shown in Figure 2d. Thus, the current blockage observed in this experiment was indeed due to the tip partially blocking the ionic current flow through the nanopore. The current was measured at 2 kHz low pass filter setting on the Axopatch 200B. The advantage of this experiment compared to G. M. King's result^[25] is that a micrometer scale blunt tip can occlude a large solid angle above the pore and can make a significant change to the nanopore access resistance. Furthermore, the significant change in resistance caused by a scanning micrometer scale tip can initially locate the position of the nanopore more quickly than a nanotube tip.

2.2. Nanopore Ionic Current Map for Pores of Different Sizes

To investigate how the SPM tip height (H_{tip}) and its radial distance from the center of the pore affect the current flow through the pore, ionic current maps, $I_s(x, y, z)$, were measured at different height ($Z = H_{\text{tip}}$) values. We first scan the area around a nanopore to know the normal vector to the surface plane, then lift the tip and scan the plane above a certain height from the surface plane. One example of an ionic current map taken at a tip height, $H_{\text{tip}} = 110$ nm, is shown in **Figure 3a**. At lifting heights above 60 nm, the drifting of the tip in the z direction is estimated to be ≈ 10 nm.^[34] At $H_{\text{tip}} = 10$ nm, the drifting problem is minimized since the feedback is on. The current blockage amplitude caused by the SPM tip, ΔI_b , was the difference between the open pore current I_0 (measured with the tip far away from the pore) and the instantaneous pore current I_s . The increase in the total pore resistance due to the tip nearby can be written as

$$\Delta R = R_s - R_0 = R_{\text{tip}} = \frac{\Psi}{I_s} - \frac{\Psi}{I_0} = R_0 \frac{\Delta I_b}{I_s} \quad (2)$$

Here $R_0 = \Psi/I_0$ is the nanopore total resistance without a SPM tip nearby, $R_s = R_0 + R_{\text{tip}} = \Psi/I_s$ is the nanopore resistance with a SPM tip nearby, $\Delta R = R_{\text{tip}}$ is the resistance increase caused by the tip blocking the flow of ions, and $\Delta I_b = I_0 - I_s$. The ratio of $\Delta R/R_0$ calculated as a function of the distance from the tip to pore center and the tip lift height H_{tip} is shown in Figure 3b for a large and long pore ($2a \approx 100$ nm, $L \approx 300$ nm), in Figure 3c for a pore its diameter is close to its length ($2a \approx 26$ nm, $L \approx 20$ nm), and in Figure 3d for a small pore ($2a \approx 7$ nm, $L \approx 20$ nm). The peak values of the normalized blockade current $\Delta I_b/I_0 = \alpha$ for data shown in Figure 3 is listed in **Table 1**. The relative resistance increase of the nanopore $\Delta R/R_0 = \alpha/(1-\alpha)$ is also listed in the table. Based on the nanopore geometry and Equation (1), the calculated ratio of the access resistance on one side of the pore $R_{\text{ac-cis}} = \rho/4a$ to R_0 , $R_{\text{ac-cis}}/R_0 = 1/[4(L/\pi a + 1/2)]$, is also given in Table 1.

The magnitude of the relative pore resistance increase $\Delta R/R_0$ (Table 1) shows that the relatively large blunt tip blocks ion flow to the pore significantly at $H_{\text{tip}} = 10$ nm along the center line of the pores. Although the same tip was used for all measurements, the peak values of the ratio $\Delta R/R_0$ at $H_{\text{tip}} = 10$ nm are 0.54, 0.18, and 0.67 for

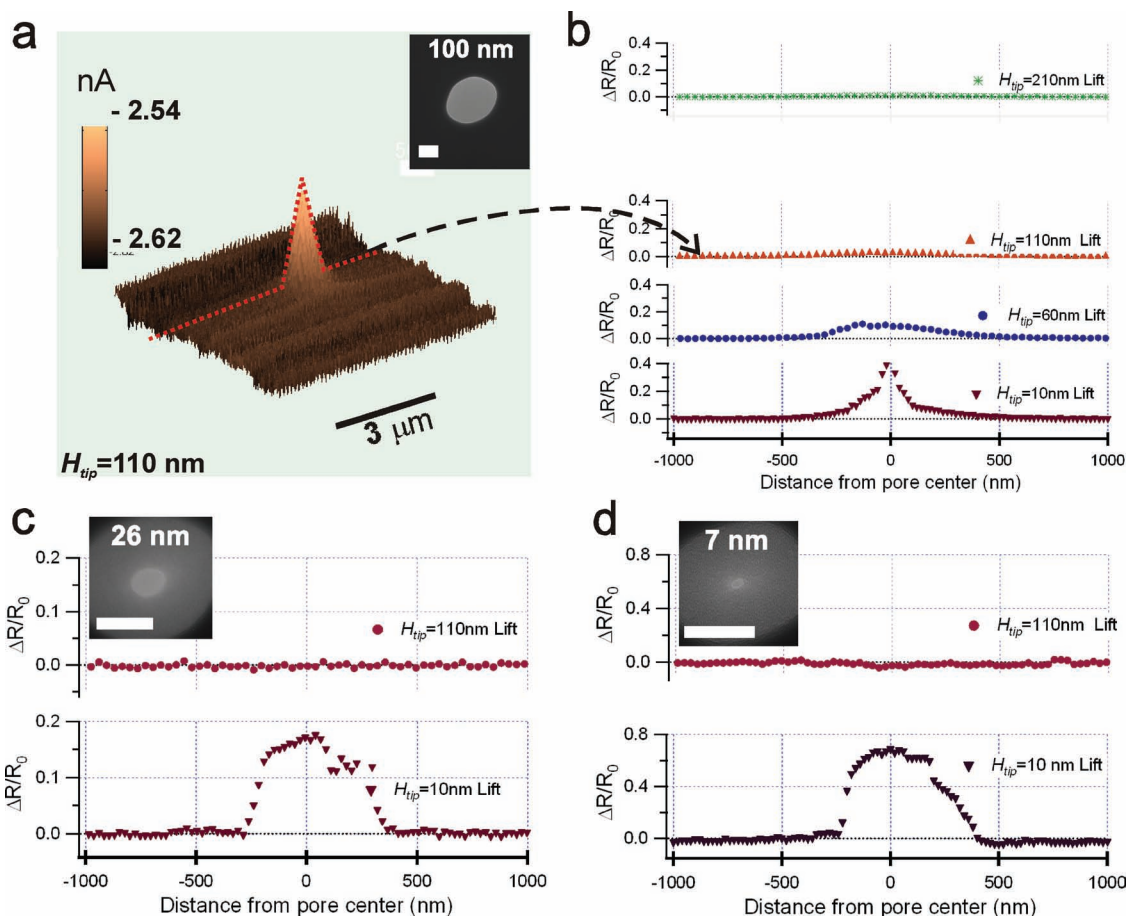


Figure 3. a) Nanopore ionic current map measured at the SPM tip height $H_{tip} = 110$ nm. A 100 nm size FIB pore was used for the measurement in 0.1 M KCl solution and $\Psi = -60$ mV. b) The ratio of $\Delta R/R_0$ as a function of the distance from the 100 nm pore in (a) measured at different tip height. The ratio of $\Delta R/R_0$ measured with a 26 nm diameter pore in 1 M KCl (c) at $\Psi = -100$ mV and with a 7 nm size pore in 1 M KCl (d) at $\Psi = -150$ mV. The insets in (b), (c), and (d) are TEM images of the scanned pores. The scale bars are 50 nm in all the TEM images. Different voltages were used to increase the ionic current signal-to-noise ratio.

pore thickness-to-radius ratios of $L/a = 6.0$ ($2a = 100$ nm), 1.5 ($2a = 26$ nm), and 5.7 ($2a = 7$ nm), respectively. This demonstrates experimentally that $\Delta R/R_0$ depends on the ratio of L/a , not the diameter $2a$, which is consistent with predictions in Equation (1) and (2) based on Ohm's law. The SPM tip height dependence of $\Delta R/R_0$ in Figure 3b shows that for the large 100 nm pore, the $\Delta R/R_0$ was still measurable at $H_{tip} = 200$ nm. A 0.2% of maximum current blockage was measured with the large diameter and long pore at the lifting height of 500 nm. In the case of small diameter pores, the pore

resistance change $\Delta R/R_0$ was not detected for lift heights over 110 nm as shown in Figure 3c,d. This is consistent with theoretical predictions that the electric field is negligible beyond a half sphere with the same radius as the pore,^[35] thus the detectable range of $\Delta R/R_0$ is expected to be shorter for pores with a smaller radius. The full width at half maximum of the pore relative resistance change profiles, $\Delta R/R_0$, are the same 0.54 μm for both the 26 nm (Figure 3c) and the 7 nm (Figure 3d) size nanopores. This is likely caused by the large dimension of the SPM tip.

Table 1. Relative current blockage, resistance change for pores measured in Figure 3 at different lift heights.

Pore size ($2a$) [nm]	Ratio of L/a	R_{ac-cis}/R_0	Measured $\Delta I_b/I_0$				Measured $\Delta R/R_0$			
			$H_{tip} =$ 10 nm	$H_{tip} =$ 60 nm	$H_{tip} =$ 110 nm	$H_{tip} =$ 210 nm	$H_{tip} =$ 10 nm	$H_{tip} =$ 60 nm	$H_{tip} =$ 110 nm	$H_{tip} =$ 210 nm
≈ 100	≈ 6	0.104	0.35	0.08	0.03	0.01	0.50	0.10	0.03	0.01
≈ 26	≈ 1.5	0.25	0.15	-	0.0	-	0.18	-	-	-
≈ 7	≈ 5.7	0.108	0.41	-	0.0	-	0.69	-	-	-

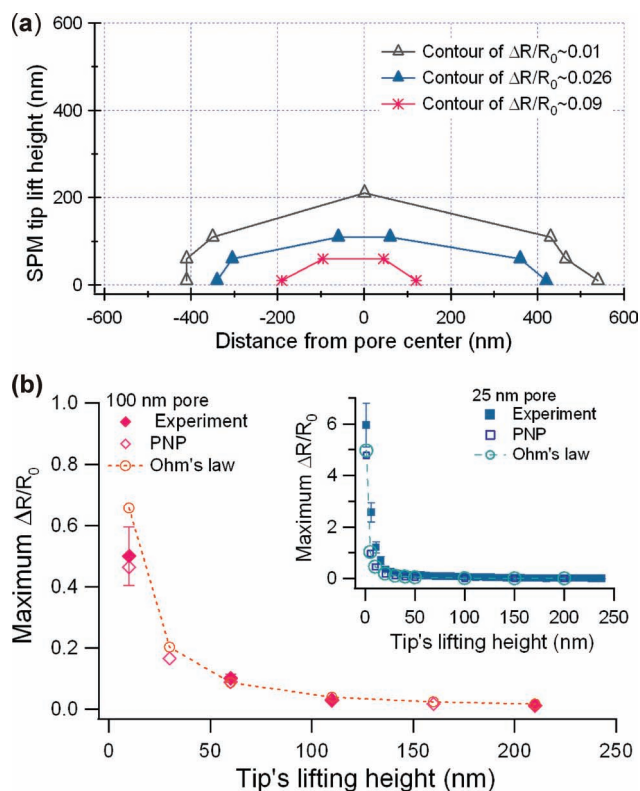


Figure 4. Contour of $\Delta R/R_0$ equal value plot measured by the SPM tip extracted from the large 100 nm pore data in Figure 3b (a). Maximum pore resistance change $\Delta R/R_0$ in experiment and simulation as a function of the lift height of a tip (b). The symbols represent experimental results for pores with diameters of 100 nm in 0.1 M KCl (◆) and 25 nm in 1 M KCl (■). The errors are the standard deviation of the Gaussian fits. The open symbols are data simulated using with PNP equations in the COMSOL Multiphysics software. The dotted lines are simulated using the same program with Ohm's law only (no surface charge).

2.3. Dependence of $\Delta R/R_0$ on Tip Location

Using the large 100 nm pore data in Figure 3b, we create a contour plot of $\Delta R/R_0$ by plotting equal values of $\Delta R/R_0$ for different tip height locations (Figure 4a). The shape of the $\Delta R/R_0$ contour is elliptical, similar to the equipotential plots for the model orifices by Gregg and Steidley.^[36]

The plot of $\Delta R/R_0$ as a function of the SPM tip height for the large ≈ 100 nm pore data in Figure 4b shows that the $\Delta R/R_0$ is approximately inversely proportional to H_{tip} , or $\Delta R/R_0 \approx 1/H_{\text{tip}}$ along the centerline of the pore.

Another measurement with a 25 nm pore in 1 M KCl with more data points (insert of Figure 4b) also shows a similar result. To measure more data points at different lifting heights, instead of scanning a whole flat plane around a pore as explained in Figure 3, we located the pore with the tip, and then lifted the tip directly at increasing values of H_{tip} while measuring ionic current. The measured maximum access resistance changes of the 25 nm diameter pore are plotted in Figure 4b (insert).

To better understand our experimental data, we simulated access resistance change ($\Delta R/R_0$) with Ohm's law and

Poisson and Nernst–Planck equations (Multiphysics from COMSOL). The details of the simulation are explained in the supporting information. Briefly, using Ohm's law or PNP equations, the access resistance can be calculated by 3D finite element simulation as shown in Figure 1a. The Nernst–Planck equation describes the motion of chemical ions in fluid. It accounts for the flux of ions under the influence of both an ionic concentration gradient (∇c_i) and an electric field ($-\nabla\Phi$).

$$J_i = -D_i \nabla c_i - \frac{z_i F}{RT} D_i c_i \nabla \Phi + c_i \mathbf{u} \quad (3)$$

Here J_i , D_i , c_i , and z_i are the flux, diffusion constant, concentration, and charged species i , respectively. Φ is the local electric potential, \mathbf{u} is the local electric potential and fluid velocity (set as zero in this work), and F , R , T are the Faraday constant, the gas constant, and the absolute temperature, respectively. The electric potential generated by chemical ions is described by the Poisson equation.

$$\nabla^2 \Phi = -\frac{F}{\epsilon} \sum z_i c_i \quad (4)$$

where ϵ is the dielectric constant of the fluid. The current passing through the pore is calculated by integrating both current densities from potassium ions and from chloride ions. The access resistance change without and with a SPM tip as described in Equation (2), $\Delta R/R_0 = (I_0 - I_s)/I_s = \frac{\int \int J_0(r) dA}{\int \int J_s(r) dA} - 1$, can be simulated with Ohm's law, or with PNP Equation (3) and (4) if charges on the nanopore surface are considered.

We plot the simulated access resistance change ($\Delta R/R_0$) versus the lifting height as shown in Figure 4b together with the experimental data. The parameters used for the simulations are: temperature $T = 298$ K, diffusion constants of potassium ion $D_K = 1.975 \times 10^{-9} \text{ m}^2 \text{ s}^{-1}$ and of chloride ion $D_{Cl} = 2.032 \times 10^{-9} \text{ m}^2 \text{ s}^{-1}$, and relative dielectric constant $\epsilon = 80$. Based on recent published work,^[12,37] we assume the geometry of the nanopores to be an hour glass shape (Figure 1a). For example, for a pore with $2a = 100$ nm and $L = 280$ nm (Figure 3b) at $\Psi = 60$ mV bias, the simulated open pore current $I_0 = -2.21$ nA. When a tip is put close to the nanopore at $H_{\text{tip}} = 110$ nm, the simulated current changed to $I_s = -2.14$ nA, therefore the simulated $(\Delta I/I_0) = 0.03$ and the total pore resistance change is $\Delta R/R_0 = 0.03$.

When the PNP model was used, the surface charge density was set at -0.02 C m^{-2} for silicon nitride nanopore surface^[31] and -0.06 C m^{-2} for the fused silica tip.^[38] At $H_{\text{tip}} = 10$ nm lifting height, the access resistance change $\Delta R/R_0$ simulated (\diamond , Figure 4b) was 39% less compared to Ohm's law (\circ). At $H_{\text{tip}} = 110$ nm, the difference between the PNP model and Ohm's law was reduced by 1%. The 39% decrease of $\Delta R/R_0$ at $H_{\text{tip}} = 10$ nm is due to the electrical double layer near the tip surface enhancing in the local solution conductivity.^[39,40] At $H_{\text{tip}} = 110$ nm, the increase in conductivity from the electrical double layer is ignorable since the double layer (≈ 1 nm) is much less than the tip height of $H_{\text{tip}} = 110$ nm.

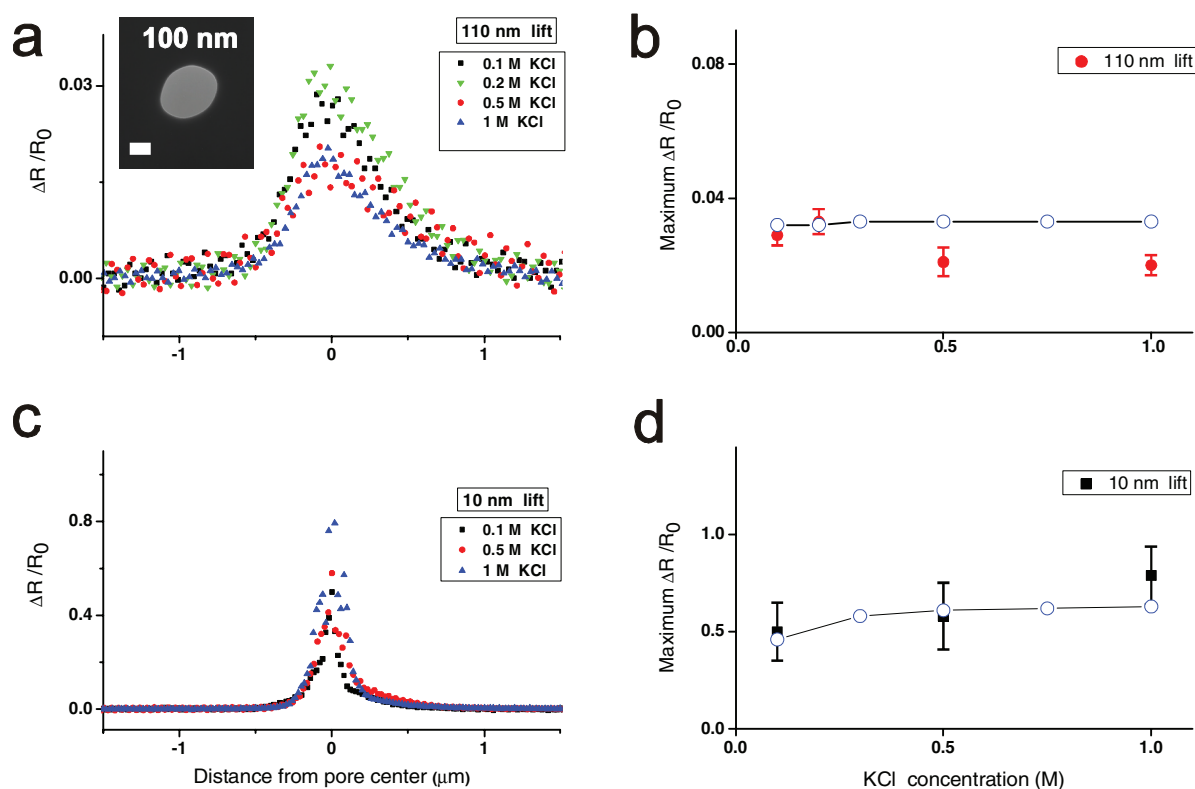


Figure 5. $\Delta R/R_0$ as a function of KCl concentration at the lift height of 110 nm (a) and 10 nm (c) from a 100 nm pore. b,d) Maximum $\Delta R/R_0$ at different KCl concentrations in (a) and (c). The bias voltage was set at $\Psi = -60$ mV for the measurement. Simulation results with PNP equations are plotted with open circles (O). The inset in (a) is the TEM image of the pore used. The scale bar is 50 nm in the TEM image.

2.4. Dependence of $\Delta R/R_0$ on Salt Concentration

Ohm's law predicts that solution conductivity does not affect the pore's relative resistance change ($\Delta R/R_0$), however, the PNP equations expect that salt concentration does affect the pore's relative resistance. We performed the same experiment with the large ($2a \approx 100$ nm) pore at different KCl concentrations while keeping the tip height H_{tip} as a constant. At $H_{\text{tip}} = 110$ nm, the $\Delta R/R_0$ distribution around the pore shown in **Figure 5a** did not change significantly at different KCl concentrations within experimental error. The maximum pore resistance change in **Figure 5b** shows the $\Delta R/R_0$ was about 0.03 as the KCl concentrations were changed.

When the tip height was kept at 10 nm, the maximum access resistance changes $\Delta R/R_0$ (**Figure 5c**) were 0.50, 0.58, and 0.79 at the KCl concentrations of 100 mM, 500 mM, and 1 M respectively. For a given height, the tip should cause the same geometric occlusion, however, at low salt concentrations surface charge effects can contribute to the local solution conductivity.^[38–40] As the salt concentration increases, the Debye length decreases. The Debye length is estimated to be ≈ 1 nm at 0.1 M KCl and ≈ 0.3 nm at 1 M KCl, so the current due to the surface charge relative to the total current is expected to increase at low salt concentrations for a tip height of 10 nm. Supporting this conclusion are numerical PNP solutions shown in **Figure 5d** that predict relative resistance changes of 0.46, 0.60, and 0.64 at the KCl concentrations of 100 mM, 500 mM, and 1 M. The surface charge contribution

was negligible at $H_{\text{tip}} = 110$ nm for both experiment and numerical PNP simulation as shown in **Figure 5b**.

3. Conclusion

In this work, we report a newly constructed apparatus that integrates solid-state nanopore ionic current measurement with a scanning probe microscope (SSN-SPM). This SSN-SPM system is capable of measuring the ionic current flow through a nanopore while a SPM tip scans the top of the pore. As the tip scans across the pore at various heights, it partially blocks the flow of ions to the pore, allowing a 3D current blockage map to be measured. Important nanopore parameters can be estimated from the 3D current blockage map: 1) how far the electric field extends above the physical boundary of the pore in 3D space, which will be useful to estimate at what distance a charged biomolecule will be captured;^[4,11] 2) the contour map of the relative resistance increase $\Delta R/R_0$ due to an increase in the pore access resistance, which has verified the access resistance concept experimentally; 3) the minimum distance from the tip to the pore at which the resistance change $\Delta R/R_0$ caused by a tip is negligible for future tethered single-molecule experiments. In addition, the $\Delta R/R_0$ maps as functions of nanopore geometry and salt concentration show that $\Delta R/R_0$ is close to zero when the tip is about five times of the pore diameter, $2a$, away from the center of the pore entrance regardless of the salt concentration investigated. The ratio of $\Delta R/R_0$ depends on L/a , on the ratio of the pore

length and its radius, and on the surface charge as the PNP equations predict. When the SPM tip is very close to the pore surface, ≈ 10 nm, our results show that the $\Delta R/R_0$ depends on salt concentration indicating a deviation from Ohm's law. Both experiment and COMSOL simulation show that the access resistance decreases inversely proportional to the tip height along the centerline of the pore.

The results reported in this work provide direct experimental measurement of access resistance of solid-state nanopores. As more research groups develop high-resolution nanopore sensing devices, access resistance becomes a more important parameter and it becomes a dominant component to the pore resistance as a pore is thinner. Access resistance is also an important parameter for understanding the DNA translocation process, for the design of future nanopore experiments, for the interpretation of current blockage data, and furthermore for the design of using nanopores to probe single DNA molecules attached to the SPM tips.

4. Experimental Section

Nanopore Fabrication: The nanopores used in this study are fabricated in a free standing silicon nitride membrane supported by 4 mm \times 6 mm silicon substrate. The thickness of the silicon nitride membrane is 275 nm and is deposited by low pressure chemical vapor deposition on both sides of the 380 μ m thick (100) silicon substrate. The freestanding membrane window is approximately 30 μ m \times 30 μ m made by procedures including photolithography, reactive ion etching, followed by anisotropic wet KOH etching. Initially, a 100 nm size pore is milled on the free standing membrane using a focused ion beam (FIB, Micrion 9500). A 3 keV noble gas Ne ion beam is used to shrink the ≈ 100 nm FIB pore to the desired pore size.^[33,41]

Measurement and Analysis: The nanopore chips are immersed in acetone and isopropyl alcohol for 30 min in series, and then are soaked in a one to one solution of ethanol and deionized water for more than a day. Electrodes are made by chloriding silver wires in bleach (Clorox). Every electrode is chlorided for one hour before measurements. The current through a nanopore is recorded by an integrated patch-clamp amplifier Axopatch 200B (Molecular Devices). The Scanning Probe Microscope stage which holds the sample holder with a nanopore chip and the headstage of the amplifier are enclosed in a Faraday cage. Recorded data are analyzed by custom routines written in MATLAB.

Supporting Information

Supporting Information is available from the Wiley Online Library or from the author.

Acknowledgements

We acknowledge discussion and helpful criticism of this work by J. Golovchenko, A. Aksimentiev, and D. Hoogerheide. We thank G.

M. King for his helpful advice and discussion about the experimental setup, and Dr. D. Gazum for his assistance in SPM setup. We also thank B. Ledden and E. Graef for nanopore fabrication and TEM imaging. This work was supported by the NIH (R21HG004776) and partially supported by NSF/MESEC (080054), ABI-1114, and NCRR/1P3ORR031154-01.

- [1] Y. Astier, O. Braha, H. Bayley, *J. Am. Chem. Soc.* **2006**, *128*, 1705.
- [2] J. J. Kasianowicz, E. Brandin, D. Branton, D. W. Deamer, *Proc. Natl. Acad. Sci. USA* **1996**, *93*, 13770.
- [3] A. Meller, L. Nivon, D. Branton, *Phys. Rev. Lett.* **2001**, *86*, 3435.
- [4] J. J. Nakane, M. Akeson, A. Marziali, *J. Phys.—Condens. Matter* **2003**, *15*, R1365.
- [5] J. Li, D. Stein, C. McMullan, D. Branton, M. J. Aziz, J. A. Golovchenko, *Nature* **2001**, *412*, 166.
- [6] A. J. Storm, J. H. Chen, X. S. Ling, H. W. Zandbergen, C. Dekker, *Nat. Mater.* **2003**, *2*, 537.
- [7] B. M. Venkatesan, B. Dorvel, S. Yemencioğlu, N. Watkins, I. Petrov, R. Bashir, *Adv. Mater.* **2009**, *21*, 1.
- [8] J. Nakane, M. Akeson, A. Marziali, *Electrophoresis* **2002**, *23*, 2592.
- [9] I. Vodyanoy, S. M. Bezrukov, *Biophys. J.* **1992**, *62*, 10.
- [10] M. Wanunu, W. Morrison, Y. Rabin, A. Y. Grosberg, A. Meller, *Nat. Nanotechnol.* **2010**, *5*, 160.
- [11] M. Gershow, J. A. Golovchenko, *Nat. Nanotechnol.* **2007**, *2*, 775.
- [12] S. W. Kowalczyk, A. Y. Grosberg, Y. Rabin, C. Dekker, *Nanotechnology* **2011**, *22*, 315101.
- [13] S. Garaj, W. Hubbard, A. Reina, J. Kong, D. Branton, J. A. Golovchenko, *Nature* **2010**, *467*, 190.
- [14] C. A. Merchant, K. Healy, M. Wanunu, V. Ray, N. Peterman, J. Bartel, M. D. Fischbein, K. Venta, Z. Luo, A. T. C. Johnson, M. Drndić, *Nano Lett.* **2010**, *10*, 2915.
- [15] G. F. Schneider, S. W. Kowalczyk, V. E. Calado, G. Pandraud, H. W. Zandbergen, L. M. K. Vandersypen, C. Dekker, *Nano Lett.* **2010**, *10*, 3163.
- [16] D. Fologea, J. Uplinger, B. Thomas, D. S. McNabb, J. Li, *Nano Lett.* **2005**, *5*, 1734.
- [17] J. Li, M. Gershow, D. Stein, E. Brandin, J. A. Golovchenko, *Nat. Mater.* **2003**, *2*, 611.
- [18] U. F. Keyser, J. v. d. Does, C. Dekker, N. H. Dekker, *Rev. Sci. Instrum.* **2006**, *77*, 105105.
- [19] U. F. Keyser, B. N. Koeleman, S. v. Dorp, D. Krapf, R. M. Smeets, S. G. Lemay, N. H. Dekker, C. Dekker, *Nat. Phys.* **2006**, *2*, 473.
- [20] E. H. Trepagnier, A. Radenovic, D. Sivak, P. Geissler, J. Liphardt, *Nano Lett.* **2007**, *7*, 2824.
- [21] H. Peng, X. S. Ling, *Nanotechnology* **2009**, *20*, 185101.
- [22] U. F. Keyser, D. Krapf, B. N. Koeleman, R. M. M. Smeets, N. H. Dekker, C. Dekker, *Nano Lett.* **2005**, *5*, 2253.
- [23] C.-C. Chen, M. A. Derylo, L. A. Baker, *Anal. Chem.* **2009**, *81*, 4742.
- [24] P. K. Hansma, B. Drake, O. Marti, S. A. Gould, C. B. Prater, *Science* **1989**, *243*, 641.
- [25] G. M. King, J. A. Golovchenko, *Phys. Rev. Lett.* **2005**, *95*, 216103.
- [26] D. M. Stein, C. J. McMullan, J. Li, J. A. Golovchenko, *Rev. Sci. Instrum.* **2004**, *75*, 900.
- [27] K. Healy, B. Schiedt, A. P. Morrison, *Nanomedicine* **2007**, *2*, 875.
- [28] B. Hille, *Ion Channels of Excitable Membranes*, 3rd ed., Sinauer Assoc., Sunderland MA, USA **2001**.
- [29] J. E. Hall, *J. Gen. Physiol.* **1975**, *66*, 531.
- [30] M. Aguilera-Arzo, V. M. Aguilera, R. S. Eisenberg, *Eur Biophys J* **2005**, *34*, 314.
- [31] H. S. White, A. Bund, *Langmuir* **2008**, *24*, 2212.

- [32] S. M. Bezrukov, I. Vodyanoy, *Biophys. J.* **1993**, *64*, 16.
- [33] J. Li, J. A. Golovchenko, in *Micro and Nano Technologies in Bioanalysis* (Eds: J. W. Lee, R. S. Foote), Human Press, Springer, New York **2009**, p.81.
- [34] J. L. Choy, S. H. Parekh, O. Chaudhuri, A. P. Liu, C. Bustamante, M. J. Footer, J. A. Theriot, D. A. Fletcher, *Rev. Sci. Instrum.* **2007**, *78*, 031101.
- [35] A. V. Sokirko, *Bioelectrochem. Bioenerg.* **1994**, *33*, 25.
- [36] E. C. Gregg, K. D. Steidley, *Biophys. J.* **1965**, *5*, 393.
- [37] M. J. Kim, B. McNally, K. Murata, A. Meller, *Nanotechnology* **2007**, *18*, 205302.
- [38] D. Stein, M. Kruthof, C. Dekker, *Phys. Rev. Lett.* **2004**, *93*, 035901-1.
- [39] D. P. Hoogerheide, S. Garaj, J. A. Golovchenko, *Phys. Rev. Lett.* **2009**, *102*.
- [40] R. M. Smeets, U. F. Keyser, D. Krapf, M.-Y. Wu, N. H. Dekker, C. Dekker, *Nano Lett.* **2006**, *6*, 89
- [41] Q. Cai, B. Ledden, E. Krueger, J. A. Golovchenko, J. Li, *J. Appl. Phys.* **2006**, *100*, 024914.

Received: July 5, 2011
Revised: September 26, 2011
Published online: December 28, 2011